Electronic Supplementary Material (ESI) for Materials Horizons.

Adhesion of impure ice on surfaces

Rukmava Chatterjee[1,2†], Rajith Unnikrishnan Thanjukutty[1,3†], Christopher Carducci[1‡], Arnab Neogi[1‡], Suman Chakraborty[1,4], Vijay Prithiv Bathey Ramesh Bapu[1,5], Suvo Banik[1], Subramanian Sankaranarayanan[1,4], Sushant Anand[1*]

[1] Department of Mechanical and Industrial Engineering, University of Illinois at Chicago, USA
[2] Carrier Corporation, 6304 Thompson Road, East Syracuse, NY, 13057, USA
[3] Abbott Molecular Inc., 1300 E Touhy Ave, Des Plaines, IL, 60018, USA
[4] Center for Nanoscale Materials, Argonne National Laboratory, Argonne IL 60439, USA
[5] ANSYS Inc., 10 Cavendish Ct, Lebanon, NH, 03766, USA

† shared first author

‡ shared second author

Email: sushant@uic.edu (S.A.)

1. Materials and Methods

Synthesis of test solutions: The chemicals tested in this study (namely sodium chloride, cesium chloride, a non-ionic surfactant Triton X-100, and ethanol) were of analytical grade or higher, purchased from Sigma Aldrich, and used in their anhydrous state without further purification. De-ionized water (>99.5% purity) was purchased from Millipore-Sigma. Aqueous solutions of these chemicals were prepared by dissolving a proportionate mass of the contaminants (varying weight percentage, wt%) in a pre-measured quantity of pure water at room conditions. The mixture container was sealed, ultrasonicated for 15 min ensuring complete dissolution, and kept fully sealed until the experimentation to prevent any external contamination.

Preparation of test samples: The test substrates used for impure ice adhesion experiments were copper (Type 110, bare and mirror-polished, McMaster-Carr), glass (McMaster-Carr), and silicon (p-type, University Wafer). They were cut into 6.5 cm^2 size and cleaned by successively sonicating them in acetone, ethanol, and isopropyl alcohol for 10 min each. Samples were then dried with nitrogen gas, plasma cleaned (Herrick Plasma Etcher) to render them superhydrophilic and tested immediately.

Protocol for impure ice adhesion measurement: The adhesion strength (τ_{adh}) of various frozen contaminants was quantified by following the "peak force" method[1] adopting the protocol outlined in our earlier works.[2, 3] Experimental validation with literature data was done by virtue of rigorous benchmarking tests on commonly tested industrial materials to confirm the reliability of our test rig and adopted experimental method. All experiments were conducted inside an environmental chamber capable of precisely controlling its ambient air temperature and relative humidity while maintaining a dust-free environment. Continuous purging of the chamber with Nitrogen gas (99% pure) established ultralow humidity (RH ≤ 3%) ambient temperature (24°C) conditions which precluded any atmospheric condensation or frosting on the test surfaces (glass, silicon, copper). These test substrates (≈1 mm thick) were thermally bonded to a sample holder (with nine slots) which was directly bolted to a Peltier surface. Contaminant solutions (sodium chloride, Triton X-100, ethanol) of varying concentrations were enclosed in 1 cm^2 square plastic cuvettes (made hydrophobic prior test) and frozen for 3 h on the test substrates using the Peltier cooler. The Peltier cold plate was controlled using a PID temperature controller to establish the desired cooling temperature. Temperature of the Peltier surface (T_{pel}) and test substrates was continuously monitored using a thermocouple (Type T, OMEGA) affixed to a reference sample of the same material. The lack of any measurable temperature difference between the ice-enclosed cuvettes and cold plate justified the accuracy of the conducted tests. Independent temperature measurements also verified the absence of any spatial temperature variation across the Peltier surface, thereby ensuring experimental uniformity. In each case, it was ensured that the solutions had completely frozen before the test. Next, the cuvette-enclosed frozen columns were pushed off very close to the test substrate (<1 mm clearance between force probe from Peltier surface) with a critical shear rate of 0.1 mm/s using a force gauge (MARK-10, accuracy=±0.1%, resolution=0.01 N) mounted on a motorized translational stage (Velmex BiSlide). This methodology ensured that the impacting force didn't introduce any bending torque in the adhesion measurements. The maximum force needed for dislodging the frozen columns was recorded for each case and the corresponding τ_{adh} was calculated by dividing this measured force by the contaminant-substrate contact area. Close-up video recording (Nikon D810 camera fitted with a TAMRON macro lens) was conducted for the entire dislodgement process & after the test the interfacial contact area was immediately scrutinized to investigate the nature of the fracture: cohesive (fracture within the bulk ice phase) or adhesive (contaminant–substrate fracture). Adopting standardized experimental controls[4] adhesion experiments were repeated at least three times per sample location for each contaminant concentration to guarantee experimental accuracy and precise repeatability of reported results. A fresh specimen (substrate & solution) was used for each test to account for batch-to-batch experimental variance.

Fabrication of ice holder for micro-computer tomography (μCT) of ice: Briny ice structure was visualized using μCT by adapting protocols outlined in previous works.[5, 6] The environment inside the μCT can reach up to 40°C. Considering that an average μCT scan can last 20 minutes, imaging briny ice is a serious challenge, necessitating adequate insulation

and an internal heat sink to maintain the ice core below 0°C. Thicker insulation with a very small thermal diffusivity delays heat flow from the environment into the ice core but may attenuate and scatter the probing X-ray beam. Hence, a balance must be struck between heat transfer performance and x-ray attenuation/scattering. To enable such imaging, we fabricated a special ice-core holder assembly made with Teflon housing, surrounded by polystyrene as outer insulation material (Figure S1a). Polystyrene has negative Hounsfield units, or a radiodensity less than that of water at standard atmospheric conditions, and an estimated thermal diffusivity of 0.124 mm^2/s, so it's well suited for the chosen purpose. Teflon tubing (~1 mm thickness) was chosen due to its thermal insulative properties (α =1.54×10^{-4} mm^2/s) and radiopacity of +650 HU at 30 kV. Lastly, the heat sinks placed at the ends of the ice cores are supercooled to pull away any additional heat that may have been transferred from the insulation or during handling in sample preparation. A series of 2.5 cm-tall Teflon cylindrical cuvettes were placed on pristine glass microscope slides. These slides were cleaned prior to placement of any particulates or dust using separate rinses of ethanol and DI water. To limit the introduction of heat from the lab environment, a board of extruded polystyrene (XPS) insulation had tube-sized holes bored through to surround the cuvettes during the freezing process. The Peltier was then dropped to the chosen supercooled temperature. Brine water of known wt% NaCl filled the cuvettes and frozen. At least two hours passed during the freezing process to ensure that the entirety of the brine solution was completely frozen.

Protocol for µCT of ice and image analysis: Once fully assembled, the 34 mm ID sample holder was placed in the µCT-scanner (ScanCo microCT 40), and an initial scout-view (Figure S1a) displays the lengthwise cross-section of the assembly. Using the SCANCO Medical µCT systems suite, a cylindrical volume of interest (VOI) of 10 mm and a diameter of 36.88 mm was selected giving a VOI of about 10,682 mm^3. The voxel size was 10 µm at an acceleration voltage of 45 kV, intensity of 177 µA, sample time of 200 ms, and rotation interval of 0.18°. For image analysis, we used ScanCo's software for manipulating raw images to remove noise and ring artifacts before thresholding them (Figure S1b). For this image analysis, the segmentation units were chosen in mg HA/ccm, the Gauss sigma value was 2.8, the Gauss support value was 6, the Lower threshold was -45.0, and the Upper threshold value was 3000.0. After thresholding, the image sequences were converted into a 3D pore map profile (Figure S1c). *Note that* existing literature for the thresholding values for concentrated salts solutions, or salts in general is sparse. One approach finds the linear attenuation coefficient of a mixture (μ) as the sum of the constituent elemental linear attenuation coefficients (μ_i) such that $\mu = \Sigma^N{}_i \, \mu_{i_a} N_i$, where N_i = [# atoms of element i]/cm^3 and $\mu_{i_a} = \mu_i / N_i$ with μ_i being dependent on the X-ray beam voltage.[7] However, since the number density of salt ions is variable and unknown in frozen precipitates of salt, the exact value of μ for Cesium Chloride (CsCl) and NaCl found in the salty ice cannot be exactly determined. Practically, then μ can be estimated directly from scan results. By adjusting the lower threshold of grayscale values such that brightly valued pixels are the only pixels made white in the binary image transform, the value of μ can be experimentally estimated for each respective salt. This method's efficacy relies on defining the soft boundary edges of salt channels, potentially introducing bias by either excluding diffused salt as noise or including bright noise as salt. In this work, the linear attenuation coefficients for CsCl and NaCl were chosen to be 1.22 and 1.05, respectively. With these respective thresholding values, the image sequences were converted into 3D salt channel profiles (Figure S1d and S1e).

Statistical analysis: The reported data were obtained through necessary normalization, whereby the obvious outliers (if any) were excluded after comprehensive experimentation and validation. All data are showcased as mean±standard deviation, with the associated error bars representing the corresponding standard deviations obtained from independent experimentation of each sample, repeated three times each (unless stated otherwise). Experimental data was analyzed in OriginPro software and plotted using Adobe Illustrator.

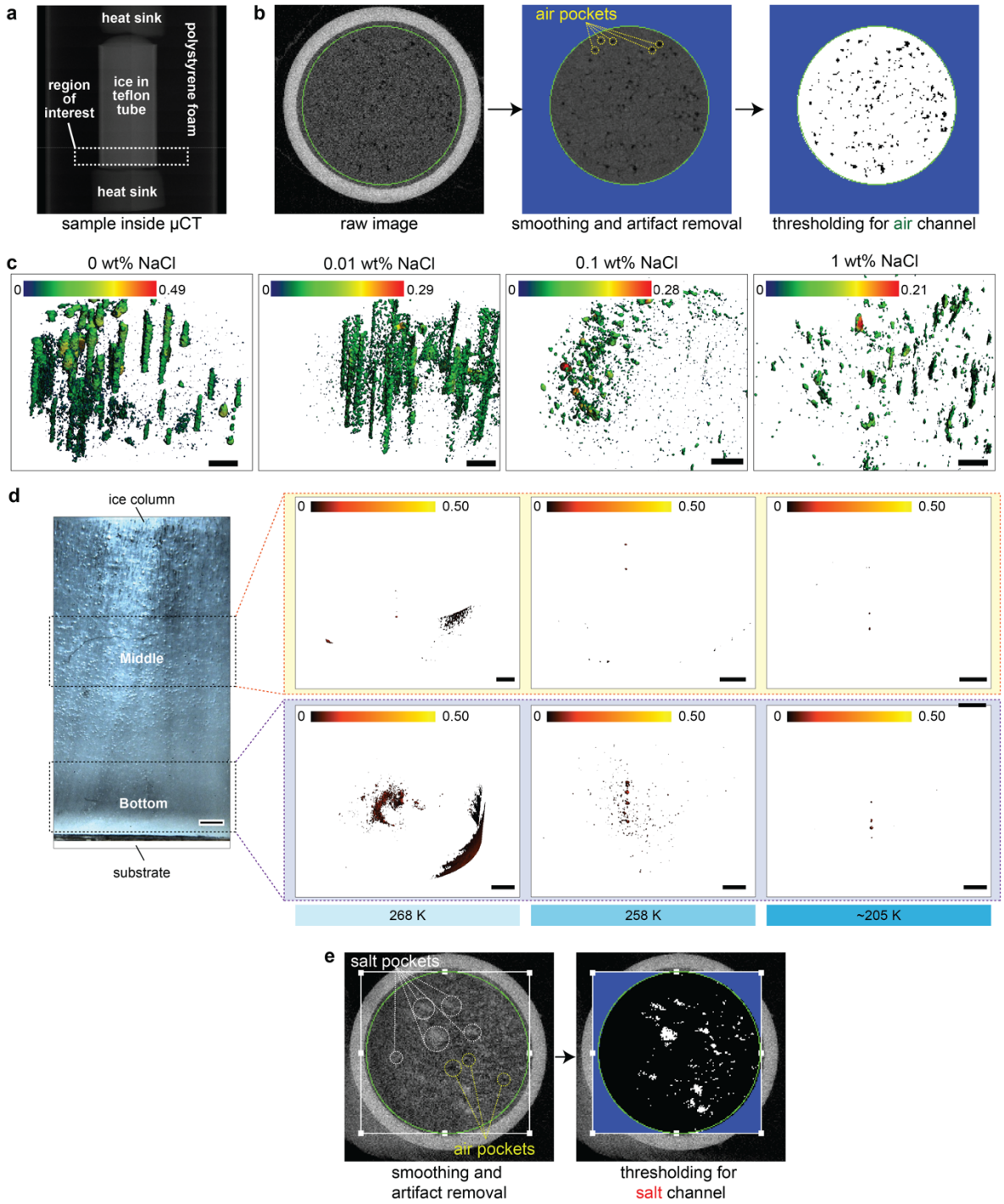

Figure S1. (a) Scout-view of the sample. **(b)** Image analysis process to threshold images to visualize air channels in ice with sodium chloride (NaCl). The dark black regions in the image show air channels. **(c)** 3D images of air channels/pores in ice at temperature of −15°C for different salt concentrations. Increasing the salt concentration decreases air pocket size and density because it leads to the formation of ice crystals with reduced space for air pockets. **(d)** Front-view image of ice formed by freezing salty water in a cuvette on a Peltier device at −15°C. Also shown are the 3D images of salt channels/pores in ice for 0.1 wt% NaCl (medium section) and 1 wt% NaCl (bottom section) at different temperatures. The air-channels for the same sections are shown in Figure 4 of the main manuscript. **(e)** Image analysis process to threshold images to visualize salt channels in ice with Cesium Chloride (CsCl). Scale bar: 1 mm. Color bar represents pore diameter (mm).

2. Molecular Dynamic (MD) simulations

Hexagonal ice (I_h) slab (with {111 terminating surface orientation) is placed on a {100} Copper (Face Centered Cubic) block acting as a wall material and the corresponding amorphization at the wall-ice interface is investigated for three different cases. The baseline simulation includes pure I_h on a copper block, the setup for which is shown in Figure S2b, the interface quasi-liquid layer (QLL) thickness is then compared with randomly infused ≈ 0.4wt % (model depicted in Figure S2a) and ≈ 1 wt% of salt (NaCl) impurities at the interface that is within 10 Å from the wall materials. The dimension of the simulation box is 46 × 26.6 × 85 Å3 which includes a vacuum region on top of the I_h slab of ≈ 17 Å.

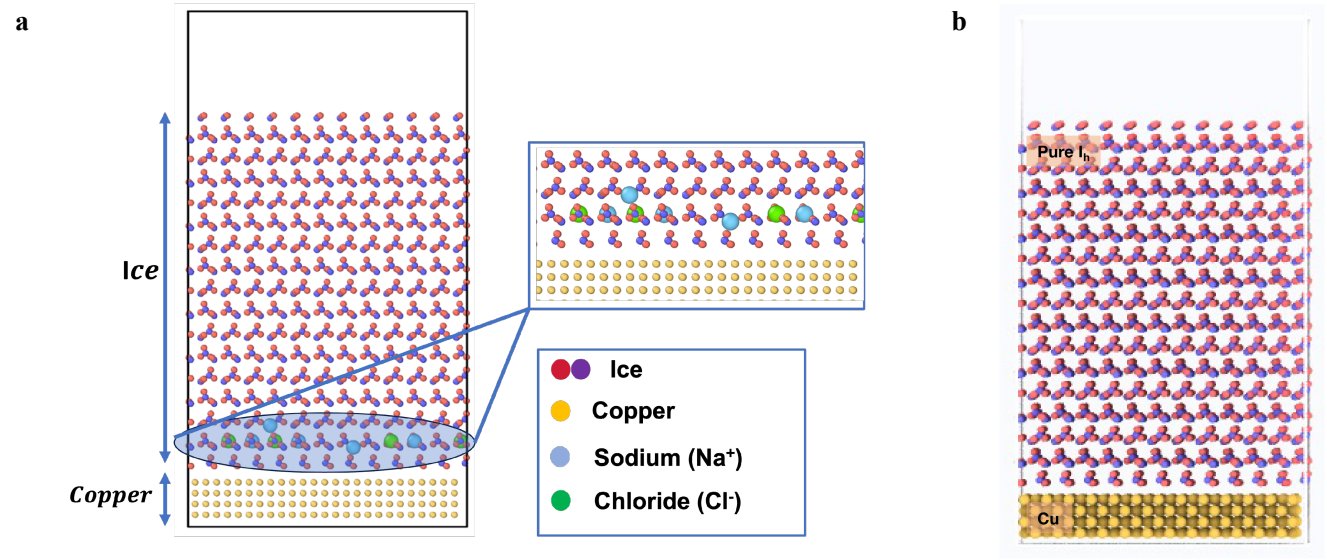

Figure S2. (a) Molecular Dynamics Setup of 0.4 wt% of NaCl doped at the interface of ice and Cu interface. **(b)** Pure ice is simulated with Cu wall for different temperatures.

The charge of oxygen and hydrogen atoms are -1.1128e and 0.5564e respectively[8] while the impurity dopants, Na^+ and Cl^- ions are assigned to have +1e and -1e and the Copper atoms are however kept neutral. The ions are randomly positioned at the Oxygen sites near the wall interface and the respective Hydrogen atoms with their related bond information are removed. The general purpose all-atom potential model TIP4P/2005 is applied to capture the water molecule interactions, the Embedded Atom Method interatomic potential is used for Cu-Cu interaction[9] and Lennard-Jones (LJ) parameters capture the cross interaction between Cu-Water[10], NaCl-Water[11] molecules. The Morse style interatomic potential is used for the cross interaction between the wall and salt ions[12]. The 12-6 LJ potential equation[13] is represented by a steep repulsive part and a smooth attractive part as a function of separation distance, $U(r) = 4\varepsilon\left[\left(\frac{\sigma}{r}\right)^{12} - \left(\frac{\sigma}{r}\right)^{6}\right]$ whereas the Morse interaction is represented by the equation $U(r) = D_0\left[e^{-2\alpha(r-r_0)} - 2e^{-\alpha(r-r_0)}\right]$, where D_0, α, and r are the potential well depth, the width of the potential well and the separation distance (<cut-off radius, r_c) respectively. The cut-off radius for the TIP4P/2005 is 13 Å and 3 Å for both LJ and Morse potential forms. The water bonds and angles are constrained by the SHAKE algorithm and periodic boundary conditions are applied in the x-y direction keeping the z boundary is fixed. The steered MD simulations are performed with the open-source platform, LAMMPS (Large-scale Atomic/Molecular Massively Parallel Simulator)[14] with each timestep of 1 fs. The system temperature is varied from 200 K to 270 K and is controlled by the combination of NVE and Langevin ensemble.

System analysis description: Chill+ algorithm: The QLL thickness at the ice-wall interface is calculated using CHILL+ algorithm based on Oxygen sites. The identification of QLL (quasi-liquid layer) involves determining partially or fully coordinated surface molecules that belong to the liquid phase. To accomplish this, we utilize the CHILL+ algorithm.[15]

The CHILL+ algorithm incorporates the correlated bond-order parameters developed by Steinhardt et al.[16] to facilitate this identification process. The local order of rank around each water molecule is determined using the aforementioned bond order parameter vectors. The principal idea is to identify staggered (S) and eclipsed (E) bonds. By utilizing this orientational order parameter, a "c" parameter is between a pair of molecules, using the equation $c(i,j) = \frac{q_i.q_j}{|q_i||q_j|}$. Where the q_i local orientational bond order parameter vector comprising of complex components around the four nearest neighbors of each molecule. A staggered bond is identified when c(i, j) ≤ −0.8, while an eclipsed bond is identified when $-0.05 \geq c(i,j) \geq -0.2$. Based on the predefined number of eclipsed and staggered bonds in hexagonal ice[15], all the crystalline particles are identified, and the remaining particles are labeled as liquid particles belonging to the QLL layer. The aforementioned CHILL+ algorithm is employed in the OVITO[17] package for the identification of the liquid particles. Subsequently, the thickness of the QLL is determined in simulations at different salt concentrations and temperatures to investigate their effects on the QLL thickness. Only the amorphization at the ice-wall interface is accounted for in the QLL width calculations.

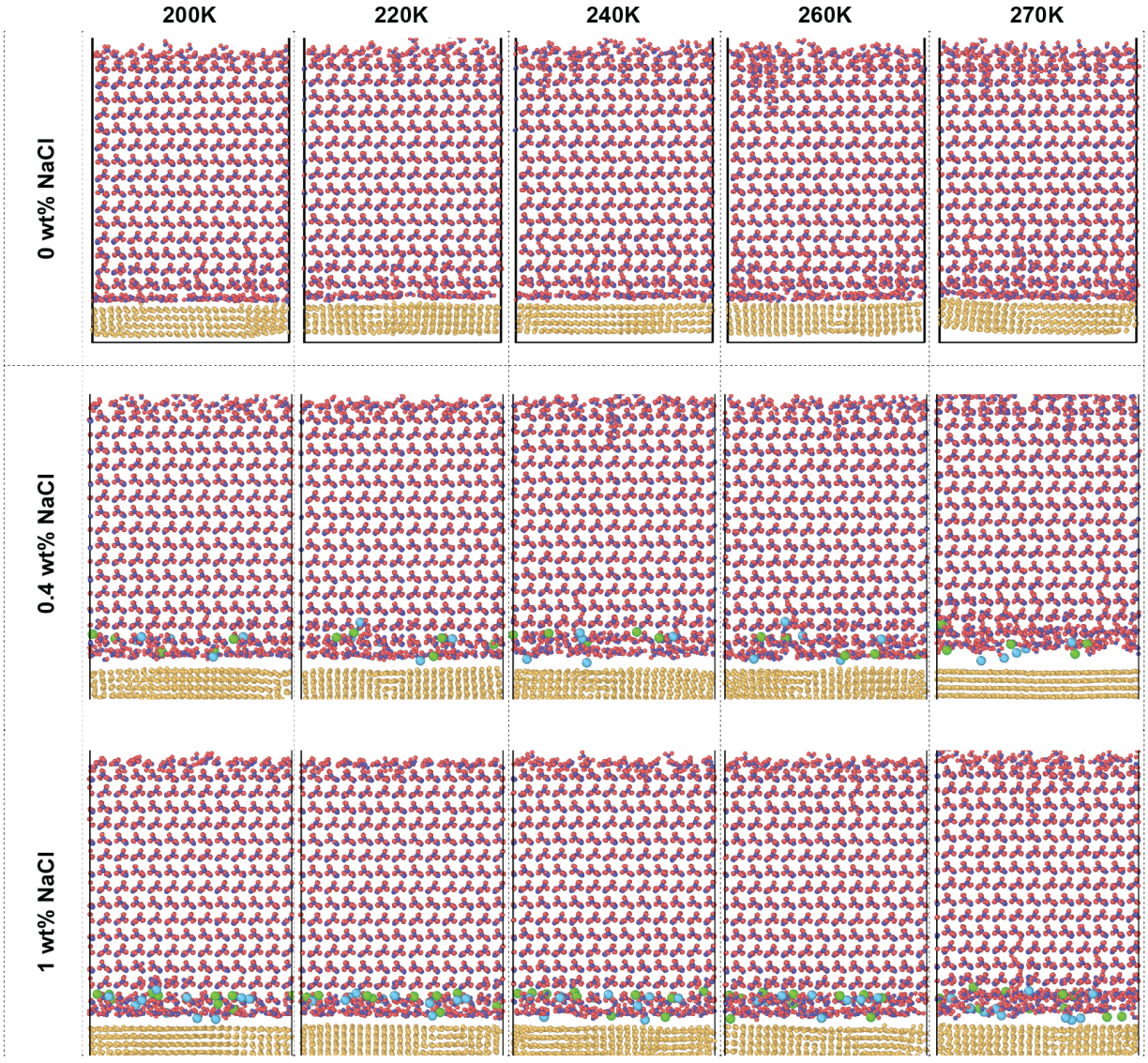

Figure S3. Results of simulations of different temperatures and salt concentrations.

REFERENCES

1. A. J. Meuler, J. D. Smith, K. K. Varanasi, J. M. Mabry, G. H. McKinley and R. E. Cohen, *ACS Appl. Mater. Interfaces*, 2010, **2**, 3100-3110.
2. R. Chatterjee, U. Chaudhari and S. Anand, *Adv. Funct. Mater.*, 2022, DOI: 10.1002/adfm.202206301, 2206301.
3. R. Chatterjee, H. Bararnia and S. Anand, *Adv. Mater.*, 2022, **34**, 2109930.
4. P. Irajizad, S. Nazifi and H. Ghasemi, *Adv. Colloid Interface Sci.*, 2019, **269**, 203-218.
5. T. Hullar and C. Anastasio, *Cryosphere*, 2016, **10**, 2057-2068.
6. R. M. Lieb-Lappen, E. J. Golden and R. W. Obbard, *Cold Reg. Sci. Technol.*, 2017, **138**, 24-35.
7. D. F. Jackson and D. J. Hawkes, *Phys. Rep.*, 1981, **70**, 169-233.
8. J. L. F. Abascal and C. Vega, *J. Chem. Phys.*, 2005, **123**.
9. S. M. Foiles, M. I. Baskes and M. S. Daw, *Phys. Rev. B*, 1986, **33**, 7983-7991.
10. T. Lin, X. Quan, P. Cheng, J. Li and G. Chen, *Int. J. Heat Mass Transfer*, 2020, **163**.
11. A. L. Benavides, M. A. Portillo, V. C. Chamorro, J. R. Espinosa, J. L. F. Abascal and C. Vega, *J. Chem. Phys.*, 2017, **147**.
12. C. G. Guymon, R. L. Rowley, J. N. Harb and D. R. Wheeler, *Condens. Matter Phys.*, 2005, **8**, 335-356.
13. J. E. Jones, *Proc. Roy. Soc. London A*, 1924, **106**, 441-462.
14. A. P. Thompson, H. M. Aktulga, R. Berger, D. S. Bolintineanu, W. M. Brown, P. S. Crozier, P. J. in 't Veld, A. Kohlmeyer, S. G. Moore, T. D. Nguyen, R. Shan, M. J. Stevens, J. Tranchida, C. Trott and S. J. Plimpton, *Comput. Phys. Commun.*, 2022, **271**.
15. A. H. Nguyen, M. A. Koc, T. D. Shepherd and V. Molinero, *J. Phys. Chem. C*, 2015, **119**, 4104-4117.
16. P. J. Steinhardt, D. R. Nelson and M. Ronchetti, *Phys. Rev. B*, 1983, **28**, 784-805.
17. A. Stukowski, *Modell Simul Mater Sci Eng*, 2010, **18**.